

Defect Contribution to the Photoluminescence from Embedded Germanium Nanocrystals Prepared by Ion Implantation and Sputter Deposition Methods

P. K. Giri¹, Kaustuv Das², and Samit K. Roy²

¹Department of Physics and Centre for Nanotechnology, Indian Institute of Technology
Guwahati, Guwahati, 781039, India

²Department of Physics and Meteorology, Indian Institute of Technology Kharagpur, Kharagpur,
721302, India

ABSTRACT

In this work, we present a comparative study of vibrational and luminescent properties of Ge nanocrystals (NCs) prepared by ion implantation (Process I) and radio frequency (RF) sputter deposition techniques (Process II). Optical Raman studies reveal presence of strain in the Ge NCs embedded in SiO₂ in both cases. Polarization dependent Raman scattering studies show that process I yields NCs with surface symmetrical Raman modes only, whereas process II yields additional surface quadrupolar Raman modes. Photoluminescence studies using 488 nm excitation show broad PL emissions peaked at ~2.3 in all the samples with varying intensities. PL studies on Ar implanted and similarly annealed SiO₂ layers confirm that the 2.3 eV emission is originated from oxygen deficient defects in the SiO₂ matrix. PL studies with 325 nm excitation show additional strong peaks at higher energies, which are believed to be due to Ge/O interface defects. It is concluded that room temperature visible light emission from embedded Ge NCs is primarily dominated by the oxygen deficient defects in SiO_x matrix and non-bridging oxygen surrounding the Ge NCs, while light emission due to quantum confined carriers in the NCs are quenched perhaps due to inherent strain in the embedded NCs.

INTRODUCTION

Embedded Ge nanocrystals (NCs) have light emitting and charge storage characteristics promising for light emitting devices and nanoscale memory devices, respectively. However, intriguing role of defects and effect of electron and phonon confinements are poorly understood in Ge NCs as compared to their counterpart in Si NCs. Experimental results have rarely met the theoretical predictions regarding the superior optical properties of Ge NCs. Several studies have indicated that the defects in the surrounding matrix are primarily responsible for broad PL in the visible region [1, 2]. Infrared photoluminescence (PL) has also been attributed to defect states in the NCs [3]. Despite the achievement of crystalline Ge NCs prepared by different methods such as ion implantation, sputtering etc, unambiguous evidence for excitonic emission from Ge NCs are lacking in the literature. This is believed to be due to the intriguing role of surface defects and strain in the NCs as well as defects in the embedding matrix.

Low frequency Raman scattering has proved to be a powerful tool to monitor surface vibrational modes of embedded NCs [4]. While the optical Raman spectra of Ge NCs of different sizes have been reported, distinctive features of Raman modes dominated by surface atoms and those dominated by interior atoms have not been identified yet. In the low-frequency range, Raman modes whose frequencies increase with decrease in NC size have been reported for various semiconductors [5, 6], and were attributed to the distortion modes of a continuum sphere.

Theoretically predicted low frequency surface vibrational modes for Ge NCs [7] have been recently verified experimentally for Ge NCs prepared by ion-implantation technique [8]. However, no studies have been reported on embedded Ge NCs prepared by sputter deposition techniques.

In this work, we have studied the light emitting and vibrational properties of embedded Ge NCs prepared by RF sputter deposition technique and ion-implantation technique. Ge NCs embedded in SiO₂ matrix are characterized by X-ray diffraction (XRD), transmission electron microscopy (TEM), Raman and photoluminescence (PL) spectroscopic techniques. Origin of the visible PL at room temperature is discussed and possible mechanism of quenching of expected PL emission from Ge NCs is pointed out.

EXPERIMENTAL DETAILS

The Ge–SiO₂ thin films were deposited on (100) oriented p-type silicon (Si) substrates by radio-frequency (RF) co-sputtering (Process I). We used a 3 inches Si target masked with Ge wafer pieces of defined area. The chamber was first evacuated to a base pressure of 1×10^{-6} Torr. The target to substrate distance was kept fixed at 6 cm and the working pressure was maintained at 0.11 Torr by introducing oxygen and argon in the ratio of 2:1. The depositions were carried out at a RF power of 50 W for 1 hour. Both sputtered silicon and germanium species while transporting through the oxygen discharge become oxidized and condense on the substrate. As-deposited samples are subsequently annealed at 700°C (Sp1) and 900°C (Sp2) for 1 hour in nitrogen ambient to grow Ge NCs of various sizes. Annealed samples were studied by XRD, TEM, PL and optical Raman and low-frequency Raman scattering (LFRS) measurements.

In the ion-implantation method (Process II), 300 keV Ge⁺ ions were implanted at room temperature on thermally grown SiO₂ films of thickness ~300 nm on Si(100) substrate with fluences 3×10^{16} (Ge1), 1×10^{17} (Ge2) and 2×10^{17} (Ge3) ions/cm². Implanted and unimplanted SiO₂ layers were first heat treated at 800°C for 1 hour and further treated at 950°C for 2 hours in argon gas ambient. Evolution of the Ge NCs has been studied after each step of annealing by using XRD, PL, Raman and LFRS techniques. For comparison, Ar ion is implanted (dose 5×10^{16} cm⁻²) on thermally grown SiO₂ layer and annealed to study PL emission caused by defects in SiO₂ layer. This sample will be referred as Ar1 for further discussion.

XRD measurements were performed in grazing incidence mode using a Powder diffractometer (Bruker D8 Advance) with a thin-film mode attachment. The TEM observations were carried out using a JEM 3000 F field emission microscope with an operating voltage of 300 kV. Raman spectra for all the samples were recorded in the backscattering geometry using vertically polarized 488 nm Argon-ion laser. Low frequency Raman spectra were recorded from 5 to 40 cm⁻¹ at steps of 0.5 cm⁻¹ using the same setup. Steady state PL measurements were made using two different laser excitations: 325 nm (He-Cd laser) and 488 nm (Ar ion laser) at room temperature.

RESULTS AND DISCUSSION

Samples prepared by process I and process II were post-annealed at various temperatures to study the evolution of the nanocrystal size and the corresponding structural and optical properties. Details of the samples are presented in Table I. The size of the nanocrystals was estimated from LFRS measurements and compared with TEM results.

TABLE I: Details of the samples used in this work.

Preparation method	Deposition time/ Ge ⁺ dose (cm ⁻²)	Annealing temperature	Sample Name	Average size of Ge NCs (nm)
RF Sputtering	1 hr	700°C	Sp1	7.3
RF Sputtering	1 hr	900°C	Sp2	9.1
Ge ⁺ implanted in SiO ₂	3×10 ¹⁶	950°C	Ge1	6.1
Ge ⁺ implanted in SiO ₂	1×10 ¹⁷	950°C	Ge2	13.0
Ge ⁺ implanted in SiO ₂	2×10 ¹⁷	950°C	Ge3	9.2
Ar ⁺ implanted in SiO ₂	5×10 ¹⁶	900°C	Ar1	--

Fig. 1 shows XRD diffraction pattern for samples Sp1 and Sp2 and the inset shows the pattern for sample Ge2. Peaks at 27.3° and 53.7° are signature of Ge NCs. In low temperature annealed sample, presence of GeO₂ along with Ge nanocrystallites are clear from the figure. At higher temperature of annealing (>900°C), Ge(111) related peak dominates the spectra. Figure 2 shows a typical TEM image (high resolution) of the embedded Ge NCs in sample Sp2. Embedded Ge NCs (dark spheres) are found to be evenly distributed in SiO₂ matrix and apparently uniform in size with nearly spherical shape, In Sp1, average size Ge NCs are expected to be smaller due to lower temperature of annealing.

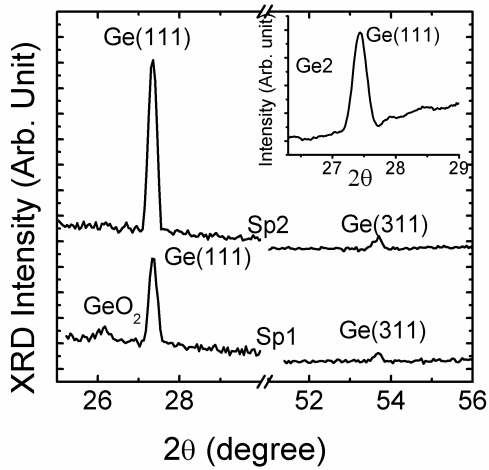


Fig. 1: XRD patter for Sp1, Sp2 and Ge2 samples showing formation of

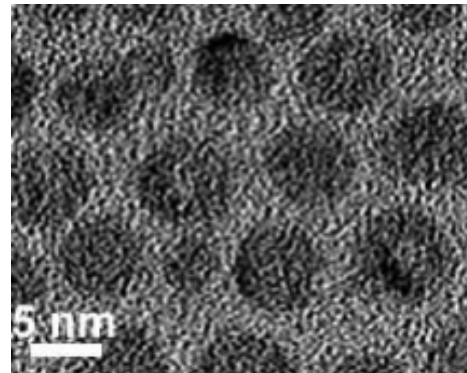


Fig. 2: A typical high resolution TEM image of Ge NCs (dark regions) embedded in SiO₂ matrix (background).

Figure 3 show typical optical Raman spectra of Sp2 showing Ge-Ge and Ge-Si Raman modes at 300 cm⁻¹ and 420 cm⁻¹, respectively. In all the samples, the Raman line width are found to be relatively broad (e.g. ~20 cm⁻¹ in Sp2) as compared to the bulk Ge crystal Raman line width (~4 cm⁻¹). The line width broadening is primarily caused by confinement of phonons in the Ge NCs. Raman line width is known to be inversely proportional to the size of the NCs. Using the phonon confinement model [9], the measured line width would corresponds to a NC size of ~4.6 nm. However, the NC sizes determined from TEM and LFRS studies (shown later) are found to be about double of this size. Hence, a part of the line width is likely to be contributed by strain in the nanocrystals caused by the surrounding matrix. The nearest neighbor distance in a-

SiO₂ is of the order of 0.16 nm and that in Ge crystals is 0.24 nm. The mismatch may result in the compressive stress on the Ge nanocrystals. The stress causes upward shift of the Ge crystalline peak thereby compensating the downward shift caused by the confinement on phonon frequency [9]. A distribution in size of the NCs may be partly responsible to account for the additional broadening. However, in the sputter deposited sample, we notice apparently uniform NC sizes. Hence, from Raman studies it is concluded that strain is present in these embedded NCs of Ge.

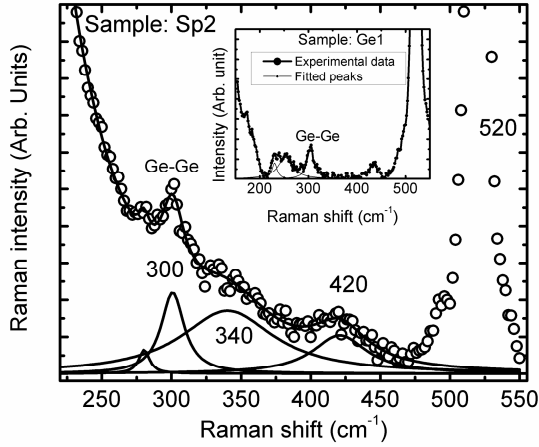


Fig. 3; Optical Raman spectra of Sp2 showing Ge-Ge modes corresponding to the formation of Ge NCs. Inset shows the Raman spectra of Ge1.

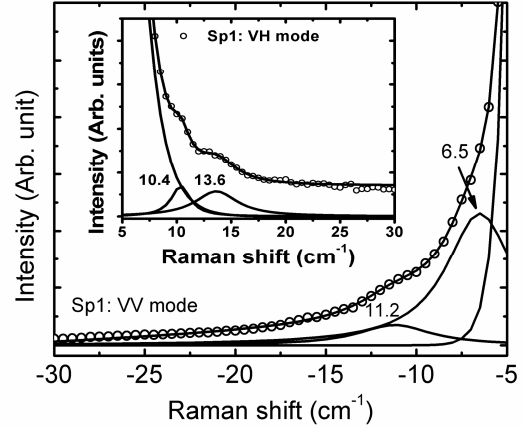


Fig. 4: LFRS spectra of Sp1 in VV mode of polarization showing peaks for NCs. Inset shows LFRS spectra recorded in VH mode of polarization.

Figure 4 shows low frequency Raman spectra for Sp1 recorded under VV polarization geometry. Inset shows spectra recorded under VH geometry. In both cases two distinct peaks are observed. It has been shown that spheroidal modes with $l=0,2$ are Raman active and torsional modes are Raman inactive [4]. The surface quadrupolar mode ($l=2$) appears in both polarized and depolarized geometry, whereas the surface symmetrical mode ($l=0$) appears only in the polarized geometry. In the present study, since the LFRS peaks appear in both VV and VH geometry, we assign the lower frequency mode to surface symmetrical (0,0) and the higher frequency mode to surface quadrupolar (0,2) modes of confined acoustic phonons as per the standard notation to denote a phonon mode [4]. Similar Raman modes have been reported recently for ZnO nanocrystals [6]. From the measured low frequency modes in Sp1, the NCs sizes are calculated as 7.3 nm using the standard formula for spheroidal mode in Ge NCs [10]:

$$\nu_0^S = 0.7 \frac{v_t}{dc} \quad (n=0),$$

where c is the velocity of light, d is the average diameter of the NCs,

and v_t is the transverse velocity of sound in Ge NCs. We have assumed a $v_t = 3.25 \times 10^5$ cm/s for Ge [10]. In Sp2 sample, the corresponding sizes grow to 9.1 nm as estimated from LFRS peak, due to the higher temperature annealing. Sizes reported in Table I are based on the LFRS analysis on Ge1, Ge2 and Ge3 as reported in Ref [8]. The estimated sizes are quite consistent with the size observed from TEM measurements as shown in Fig.2. Any deviation in the results would be expected for non-spherical shapes of the NCs and assumption of appropriate boundary

conditions. Therefore, measurement of acoustic phonon modes allows a fair assessment of the size and shape of the NCs and thus a powerful nondestructive technique to characterize nanocrystals. Note that in Ge1–Ge3 samples, we observed LFRS peaks only in VV configuration [8], and the peaks were attributed to surface symmetrical (0,0) spheroidal mode. This is in contrast to the case of Sp1 and Sp2 samples, where we observe both symmetrical (0,0) mode and quadrupolar (0,2) mode. This is believed to be due to different surrounding of the NCs prepared by two different methods. In two cases the Ge/SiO₂ interface is expected to be different due to different processing conditions. In the case of ion implanted method, lattice damage induced strain in the SiO₂ matrix may be forbidding the surface quadrupolar mode to be observed.

Figure 5 shows room temperature PL spectra of Sp1, Sp2 and Ge2 samples with laser excitation of 488 nm. The sputter deposited samples show a broad and weak peak at ~545 nm and the ion-implantation induced samples (e.g. Ge1, Ge2 and Ge3) show a broad but relatively strong peak at ~533 nm. Since the peak position is almost independent of the size of the NCs and the sample preparation conditions, the PL emission is not produced by the radiative recombination of excitons confined in the Ge NCs. In the literature, similar peaks at ~540 nm are attributed defects in SiO₂ (i.e. nonbridging oxygen hole centre) [2]. In fact, our Rutherford backscattering studies on Ge ion-implanted SiO₂ (thermally grown) samples showed that implanted and annealed SiO₂ layers are oxygen deficient i.e. it becomes SiO_x, where $x < 2$. Hence, we attribute the visible broad peak shown in Fig. 5 to oxygen deficient defects in the SiO₂ matrix.

To further confirm the contribution of defects in the visible PL, sample Ar1 is studied along with other samples under identical conditions. Figure 6 shown PL spectra excited with 325 nm for samples Sp1, Sp2 and Ar1. In addition to the peak near 545 nm, we observe several additional PL peaks at lower wavelength (higher energy) in these samples. Under 325 nm excitation, samples Sp1, Ar1 have common peaks at ~401 nm and ~510 nm. Hence, these peaks cannot be attributed to emission from Ge NCs. Peaks at 401, 510 and 545 nm are attributed to

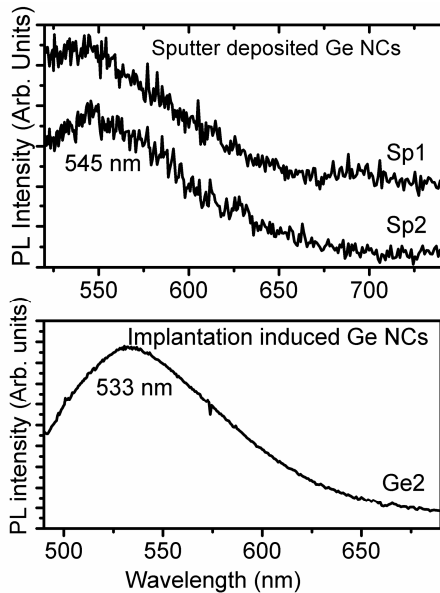


Fig. 5: Room temperature PL spectra of Sp1, Sp2 and Ge2 samples. Laser excitation at $\lambda_{ex} = 488.0$ nm.

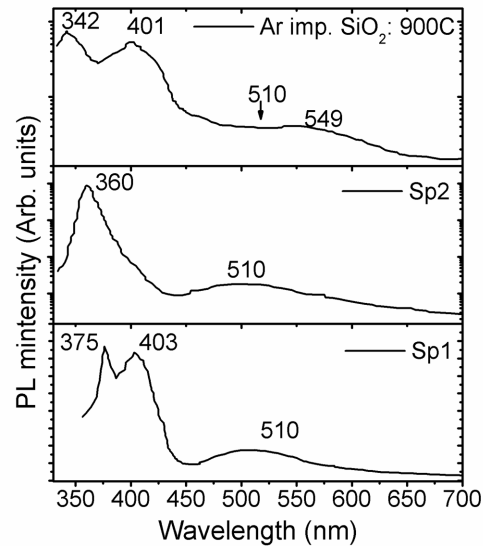


Fig. 6: Room temperature PL spectra of sample Sp1, Sp2, Ar1 with 325 nm excitation.

defects in the matrix surrounding the Ge NCs. Since the 401 nm PL peak is observed in Ar1 where no Ge NCs are present, it cannot be related to GeO_x surrounding the Ge NCs. This is contrary to the assignment of blue PL to Ge/O related defects in sputter deposited Ge NCs studied in Ref [2]. It is likely that the quality of the SiO_x ($x < 2$) surrounding the Ge NCs is different in all the samples prepared under different conditions. We propose that a large number of highly distorted bonds in the inhomogeneous strain field of Ge/SiO_x interface are responsible for the appearance of the UV emission in these annealed samples. In samples Sp1 and Sp2, the peaks at 375 nm and 360 nm are likely to be related to Ge/O-related defects at the nanocrystal/oxide interface [11]. It may be noted that despite the presence of well-formed spherical Ge NC in these sample, visible PL could not be related to the radiative recombination of excitons confined in the Ge NCs. We believe that this is primarily related to the strain field in the interior of the small NCs and the unavoidable surface defects at the NCs that are embedded in the SiO_x matrix. The lattice strain may be responsible for nonradiative recombination at the NCs and hence the expected PL due to quantum confined excitons is quenched by such defects.

CONCLUSION

In conclusion, comparative studies on embedded Ge NCs formed by sputter deposition and ion-implantation show that Ge NCs of the size range 6-13 nm are formed in different samples. Optical Raman studies reveal the presence of strain in the Ge NCs. LFRS studies show only surface symmetrical acoustic phonon modes of Ge NCs in implanted samples, whereas sputter deposited NCs show surface symmetrical and surface quadrupolar acoustic phonon modes in Ge NCs. PL studies with different excitation wavelength show that the visible PL emission primarily originates from oxygen deficient defects in the surrounding SiO_x matrix and Ge/O related interface defects. It is proposed that the radiative recombination of excitons confined in Ge NCs is inhibited due to the inherent strain in the embedded NCs.

REFERENCES

1. K. S. Min, K. V. Shcheglov, C. M. Yang, H. A. Atwater, M. L. Brongersma, A. Polman, *Appl. Phys. Lett.* 68, 2511 (1996).
2. M. Zacharias and P. M. Fauchet, *Appl. Phys. Lett.* 71, 380 (1997).
3. X. L. Wu, T. Gao, G. G. Siu, S. Tong, X. M. Bao, *Appl. Phys. Lett.* 74, 2420 (1999).
4. E. Duval, A. Boukenter, and B. Champagnon, *Phys. Rev. Lett.* 56, 2052 (1986).
5. A. Tanaka, S. Onari, and T. Arai, *Phys. Rev. B* 47, 1237 (1993).
6. H. K. Yadav, V. Gupta, K. Sreenivas, S. P. Singh, B. Sundarakannan, and R. S. Katiyar, *Phys. Rev. Lett.* 97, 085502 (2006).
7. W. Cheng, S. Ren, and P. Y. Yu, *Phys. Rev. B* 68, 193309 (2003).
8. P.K. Giri, R. Kesavamoorthy, B.K. Panigrahi and K.G.M. Nair, *Solid State Comm.* 136, 36 (2006).
9. X.L. Wu, T.Gao, X.M. Bao, F. Yan, S.S. Jiang, and D. Feng, *J. Appl. Phys.* 82, 2704 (1997).
10. N. N. Ovsyuk, E. B. Gorokhov, V. V. Grischenko, and A. P. Shebanin, *JETP Lett.* 47, 298 (1988).
11. L. P. Ginzburg, A. A. Gordeev, A. P. Gorchakov, and A. P. Jilinsky, *J. Non-Crys. Solids* 183, 234 (1995).